Rev. Int. Contam. Ambie. 38 (Sustainable Architecture and Urban Environment) 59-80, 2022
https://doi.org/10.20937/RICA.54407

STUDY ON EQUIVALENT FRACTURE TOUGHNESS OF RECYCLED STEEL FIBER-REINFORCED CONCRETE BASED ON DIGITAL IMAGE CORRELATION TECHNOLOGY

Estudio sobre la dureza de la fractura equivalente de concreto reforzado con fibras metálicas recicladas con base en la tecnología de correlación digital de imágenes

Yan LI[1], Rong-Hua ZHAO[1], Wen-Yang DONG*[2] and Geng CHEN[1]

[1] School of Civil Engineering, Jilin Jianzhu University, Changchun, Jilin Province, China.
[2] Computer Science and Technology Engineering Center, The 964th Hospital, Changchun, Jilin Province, China.

*Author for correspondence: delwine@126.com

(Received May 2021, accepted September 2021)

Key words: recycled steel fiber-reinforced concrete, three-point bending beam, digital image correlation technology, equivalent fracture toughness, extended finite element method

ABSTRACT

Recycled steel fiber-reinforced concrete is a new hybrid high performance environmental protection composite material, which can be widely used in the construction industry and provide a new research direction for national green and sustainable development. In this study, three-point bending beams with a prefabricated incision were used to evaluate the fracture performance of plain concrete, steel fiber-reinforced concrete and recycled steel fiber-reinforced concrete with different fiber volume contents, fiber length-diameter ratios and relative incision depths based on digital image correlation technology. The results show that recycled steel fibers can improve the crack resistance of concrete beams better than ordinary steel fibers; The crack resistance of specimens increases with the increases of volume ratio of recycled steel fibers, and when the fiber content is from 0.0% to 1.0%, the increased amplitude of the crack resistance of specimens increases gradually, when the fiber content is from 0.5% to 1.0%, the increased amplitude of the crack resistance of specimens reaches the maximum, and when the fiber content is from 1.0% to 1.5%, the increased amplitude of the crack resistance of specimens decreases; The crack resistance of specimens increases with the increases of length-diameter ratio of recycled steel fibers, and when the fiber length-diameter ratio is from 30 to 50, the crack resistance of specimens increases relatively large, when the fiber length-diameter ratio is from 50 to 70, the crack resistance of specimens increases relatively small; The crack resistance of specimens decreases with the increases of relative incision depth of specimens, and when the relative incision depth is from 0.2 to 0.3, the crack resistance of specimens decreases relatively large, when the relative incision depth is from 0.3 to 0.4, the crack resistance of specimens decreases relatively small; The equivalent fracture toughness of concrete beams does not change with the changes in the relative incision depth. The simulated results correlated well with the experimental results, except some macroscopic phenomena during the cracking process. This study can provide references for the research of fracture behavior of steel fiber-reinforced concrete materials and the recycling of steel wire from waste tires.

Palabras clave: concreto reforzado con fibras metálicas recicladas, flexión de vigas en tres puntos, tecnología de correlación digital de imágenes, dureza de fractura equivalente, método de extensión de elemento finito

RESUMEN

El concreto reforzado con fibras de acero recicladas es un nuevo material híbrido de alto desempeño en la protección ambiental que puede ser utilizado de manera amplia en la industria de la construcción y proporcionar nuevas direcciones en la investigación para el desarrollo nacional verde y sustentable. En este estudio se utilizaron vigas con tres puntos de flexión, con una incisión prefabricada, para evaluar el comportamiento de fractura del concreto común, del concreto reforzado con fibras de acero y del concreto reforzado con fibras de acero recicladas; se utilizaron diferentes volúmenes de fibras, de tasas diámetro longitud y de profundidades relativas de incisión empleando tecnología de correlación de imágenes. Los resultados muestran que las fibras de acero recicladas incrementan la resistencia a la fractura de las vigas en comparación con las fibras de acero ordinarias. La resistencia de los especímenes se incrementa con la tasa de volumen de las fibras recicladas. Cuando el contenido de fibras está entre 0.0 y 1.0% la resistencia aumenta gradualmente, cuando está entre 0.5 y 1.0% se alcanza la máxima resistencia a las fracturas y cuando se encuentra entre 1.0 y 1.5% la resistencia disminuye. La resistencia se incrementa con la tasa longitud diámetro de las fibras recicladas. Cuando se encuentra entre 30 y 50 la resistencia de los especímenes se incrementa de manera relativamente grande, cuando está entre 50 y 70 el incremento es relativamente pequeño. En relación con la profundidad de incisión relativa la resistencia disminuye. Cuando está entre 0.2 y 0.3 disminuye de manera relativamente grande y entre 0.3 y 0.4 lo hace de manera relativamente pequeña. La dureza de fractura equivalente de las vigas de concreto no cambia con las variaciones en la profundidad de incisión relativa. Los resultados simulados se correlacionan bien con los experimentales, excepto por algunos fenómenos macroscópicos durante el proceso de fractura. Esta investigación puede proporcionar referentes para la investigación sobre el comportamiento de las fracturas de concreto reforzado con fibras de acero y sobre el reciclaje de alambre de acero de neumáticos de desecho.

INTRODUCTION

Concrete is widely used because it is easy to form and use, economical and environment-friendly, has good durability and other advantages, but it still has shortcomings in tensile and flexural resistance, plastic and other aspects. Although lightweight concrete made by adding waste tire particles into concrete as additives can improve the bending toughness, impact resistance, fatigue resistance, and frost resistance of concrete, it will reduce the strength and elastic modulus of concrete (Huang et al. 2004, Chen and Liu 2014). Furthermore, it cannot eliminate the shortcomings of low tensile strength of concrete. The steel fiber-reinforced concrete made by adding a certain proportion of steel fiber into concrete has strong bending, tensile, shear, and crack resistances and can be widely used in practical projects. After many years of research on its strengthening mechanism, two theoretical achievements have been made. One is the composite material mechanics theory (Liu et al. 2018), and the second is the fiber spacing theory (Nourmohammadi et al. 2020). As a composite material with excellent mechanical properties, engineers worldwide favor steel fiber-reinforced concrete (SFRC).

The recycled steel fibers formed by compressing steel wire from waste tires also has an excellent performance in tensile strength, yield strength, and other mechanical properties (Peng et al. 2015). Although its price is like or slightly higher than ordinary steel fibers, as the volume of ordinary steel fibers is small, the amount of ordinary steel fibers under the same volume ratio is much more than that of recycled steel fibers. Therefore, using recycled steel fibers in engineering is more economical and reasonable than ordinary steel fibers. According to incomplete statistics, in China, there are as many as 1.4 billion

tires scrapped annually for several reasons, and the number of waste tires in the world exceeds 2.5 billion, with a total mass of more than 20 million tons. Currently, harmless use of waste tires in China mainly includes renovation treatment, production of rubber powder, and regeneration of rubber for tire powder. The wire accounts for about 14% of the weight of the total tire, and its composition is mostly cold-drawn steel. After being recycled as steel, it is mixed into concrete with a fiber composite material, solving the problems of underutilization of waste tire resources and environmental pollution and may have a wide application prospect in civil engineering (Carrillo et al. 2020).

RESEARCH BACKGROUND

Hecacob, an expert from the Soviet Union, first developed SFRC (Barros and Figueiras 1999). Since then, studies on the mechanical properties of SFRC have been conducted in various countries around the world. Sun et al. (2019) evaluated the fracture performance of basalt fiber-reinforced concrete-incision beams by using the three-point bending (TPB) test method. The results showed that the increases in basalt fiber content can significantly improve the fracture performance and toughness of concrete beams, and the numerical simulation results correlate well with the experimental results. Simalti et al. (2021) studied the compressive, split tensile, and flexural performance of ordinary self-compacting concrete, self-compacting concrete containing manufactured steel fibers and self-compacting concrete containing recycled steel fibers. The results show that when the volume ratio of steel fibers is 1.5%, the self-compacting concrete containing recycled steel fibers has better overall performance than the other two kinds of concrete, and is more economical and environmentally friendly. Lakavath et al. (2019) studied the influence of steel fibers on the shear performance of prestressed concrete beams by using digital image correlation (DIC) technology. The results show that the crack resistance of concrete beams enhanced after the steel fibers added. In China, the application and research of concrete began in the 1970s, Cao et al. (2013) conducted experimental research on the fracture performance of TPB incision-fiber-reinforced concrete beams, and the results showed that with the increases in fiber content, the compressive and splitting strengths of fiber-reinforced concrete beams would be reduced, whereas the cracking resistance would be significantly improved. Xu et al. (2008) proposed the double-K fracture parameters that can reflect the characteristics of concrete cracks development according to their experimental observations and proposed their analytical expressions. The results show that the two-fracture toughness of concrete can describe the characteristics of concrete cracks development more accurately.

However, the above studies predominantly focus on the fracture performance analysis of plain concrete and ordinary steel fiber-reinforced concrete. There is no comparative analysis on the fracture performance differences between ordinary SFRC and recycled SFRC. The influence of fiber types, such as fiber length-diameter ratio, on the fracture performance of steel fiber-reinforced concrete beams is not studied in detail. There is also a lack of research on the influence of relative incision depth on the crack resistance of concrete specimens, such as the TPB incision beam, which is easy to manufacture, simple to operate, reliable to measure, and suitable for testing the fracture performance of concrete specimens under conventional conditions. This study evaluated the fracture behavior of plain concrete and steel fiber-reinforced concrete by using TPB beams with prefabricated incisions. Cracking and fracturing loads were measured by using digital image correlation technology (Skaryński et al. 2013, Liu et al. 2020), and the equivalent fracture toughness was calculated by using the analytical method of the fictitious crack model. Furthermore, the differences of fracture properties between ordinary SFRC and recycled SFRC and the differences of fracture properties of steel fiber-reinforced concrete with different fiber volume contents, fiber length-diameter ratios, and relative incision depths are compared. The study can provide references for researching on the fracture behavior of steel fiber-reinforced concrete materials and the recycling of wire from waste tires (Li et al. 2020).

EXPERIMENTAL PROGRAMS AND RESULTS ANALYSIS

Experimental materials

The rubber and rust on the surface of recycled steel fibers (the steel wire from waste tires) were removed in the laboratory. The diameter of fibers is 1.5 mm, the tensile strength is 1800 MPa. To ensure the effective bonding length between recycled steel fibers and concrete (Ming et al. 2020), many experts and scholars have conducted in-depth studies and found that recycled steel fibers with length-diameter ratio above 30 can play the bridging role with concrete

better. Therefore, recycled steel fibers with length-diameter ratio above 30, 50, and 70 were adopted in this experiment.

Design of specimens

In **figure 1a**, S is the span of the beam. For selecting the specification and size of steel fiber-reinforced concrete TPB beams, the size of specimens is finally determined as L × W × H = 550 mm × 150 mm × 150 mm following the Standard for Testing Methods for Mechanical Properties of Ordinary Concrete (GB/T 50081-2002) and on the basis of a comprehensive literature review (Yin et al. 2019).

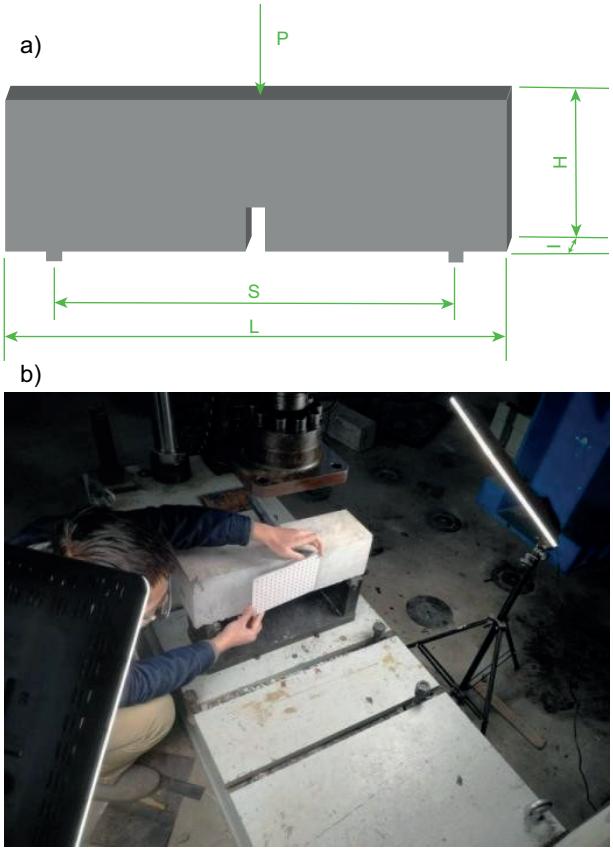

Fig. 1. The test of TPB beams, a) Model of the TPB beam; b) The test process of TPB beams.

In this test, the strength grade of concrete is C40, and thirty-six groups of TPB beam specimens were poured, with two specimens in each group, including three groups of ordinary concrete beams, six groups of concrete beams mixed with ordinary steel fibers, and the rest were concrete beams mixed with recycled steel fibers. Furthermore, six additional TPB beam specimens were poured as data supplements. The four types of fiber volume contents in specimens were 0.0%, 0.5%, 1.0%, and 1.5% (Liao et al. 2020). The three types of relative incision depths of concrete beams were 0.2, 0.3, and 0.4. During the test, the fibers were uniformly distributed in the concrete matrix (Raju et al. 2020).

Determination of cracking loads and fracturing loads

The test equipment was an electro-hydraulic servo universal machine. When loading, after adjusting the position of TPB beams, the DIC light was turned on, the camera position was adjusted and focused, and the screen test area was adjusted from light blue to purple. Cameras were calibrated with appropriate calibration plates, and 15-30 calibration image groups were taken. In addition to the loading device, other performance indexes were measured and analyzed in the test process of steel fiber-reinforced concrete specimens. **Figure 1b** shows the test process of TPB beams. In this test, DIC technology was combined with the resistance strain gauge method (Xu et al. 2015). During the test, the cracking loads of TPB beams were measured by placing resistance strain gauges 1 cm at both ends of the prefabricated incision. After the loading started, the energy of the recycled SFRC gradually concentrated on both ends of the prefabricated incision. Simultaneously, the strain on both sides of the prefabricated incision increased, and the p-ε curve showed a nearly straight upward trend. After reaching the peak point, the p-ε curve retracted. According to the analysis of variation trend of curve p-ε, the microcracks began to appear in the strain gauge measuring point area when the peak point came, and the concrete cracked at this time, the accumulated energy of the recycled SFRC was also released. At this point, the p-ε relation curve turned, and this turning point was called the cracking load (P_{ini}). When the strain changes dramatically, the TPB beam specimen reached the maximum bearing capacity before fracture, and the load was the fracturing load (P_{max}). The test results show that the test data measured by using the resistance strain gauge method and the data measured by DIC technology were close to each other. **Table I** presents the cracking and fracturing load values of TPB beam specimens.

In **table I**, TPB-05-30-02- represents the volume content of ordinary steel fibers in a TPB concrete beam specimen is 0.5%, the length-diameter ratio of ordinary steel fibers is 30, and the relative

TABLE I. CRACKING AND FRACTURING LOAD VALUES OF TPB BEAM SPECIMENS (UNIT: kN).

No.	Cracking load values	Fracturing load values	No.	Cracking load values	Fracturing load values
TPB-00-02	9.5	14.3	TPB-05-50-02	14.7	19.5
TPB-00-03	6.7	9.6	TPB-05-50-03	10.4	14.1
TPB-00-04	4.6	6.9	TPB-05-50-04	7.2	10.0
TPB-05-30-02-	11.6	15.9	TPB-10-50-02	20.6	25.9
TPB-05-30-03-	8.3	11.4	TPB-10-50-03	14.9	19.5
TPB-05-30-04-	5.5	7.9	TPB-10-50-04	10.7	14.5
TPB-10-50-02-	17.9	23.4	TPB-15-50-02	26.6	30.4
TPB-10-50-03-	12.7	17.4	TPB-15-50-03	18.9	23.8
TPB-10-50-04-	9.1	12.8	TPB-15-50-04	13.6	18.4
TPB-05-30-02	13.1	17.7	TPB-05-70-02	15.7	20.8
TPB-05-30-03	9.3	12.7	TPB-05-70-03	11.1	14.9
TPB-05-30-04	6.2	8.9	TPB-05-70-04	7.9	10.7
TPB-10-30-02	18.2	23.5	TPB-10-70-02	22.3	27.8
TPB-10-30-03	12.9	17.6	TPB-10-70-03	16.2	20.8
TPB-10-30-04	9.6	13.3	TPB-10-70-04	11.5	15.3
TPB-15-30-02	22.7	28.1	TPB-15-70-02	28.1	31.8
TPB-15-30-03	16.2	22.1	TPB-15-70-03	20.9	24.9
TPB-15-30-04	12.6	17.2	TPB-15-70-04	14.4	19.3

incision depth of the specimen is 0.2. TPB-05-30-02 represents each parameter of a TPB concrete beam specimen with recycled steel fibers. The statistical analysis was made on $P_{ini} / P_{\max}$ of TPB beam specimens in this experiment, and the approximate range was between 0.65 and 0.87.

Calculation of equivalent fracture toughness

According to the fracture characteristics of concrete quasi-brittle materials, the equivalent fracture toughness of various concrete materials was calculated in **table II** by using the analytical method based on the fictitious crack model (Li and Liu 2006).

TABLE II. EQUIVALENT FRACTURE TOUGHNESS VALUES OF TPB BEAM SPECIMENS (UNITS: $MPa \cdot m^{1/2}$).

Numbers	a_c / mm	$\widetilde{K}_{IC}$	Numbers	a_c / mm	$\widetilde{K}_{IC}$
TPB-00-02	43.4	1.20	TPB-05-50-02	46.7	1.77
TPB-00-03	58.3	1.18	TPB-05-50-03	57.4	1.77
TPB-00-04	63.2	1.17	TPB-05-50-04	67.3	1.76
TPB-05-30-02-	43.2	1.38	TPB-10-50-02	51.3	2.49
TPB-05-30-03-	53.7	1.36	TPB-10-50-03	57.3	2.48
TPB-05-30-04-	61.2	1.35	TPB-10-50-04	64.7	2.47
TPB-10-50-02-	46.9	2.23	TPB-15-50-02	53.2	3.04
TPB-10-50-03-	54.6	2.22	TPB-15-50-03	58.5	3.03
TPB-10-50-04-	61.1	2.21	TPB-15-50-04	62.6	3.02
TPB-05-30-02	42.9	1.54	TPB-05-70-02	47.6	1.92
TPB-05-30-03	52.1	1.53	TPB-05-70-03	57.1	1.91
TPB-05-30-04	61.1	1.51	TPB-05-70-04	67.4	1.89
TPB-10-30-02	49.1	2.20	TPB-10-70-02	49.8	2.72
TPB-10-30-03	56.5	2.19	TPB-10-70-03	57.2	2.71
TPB-10-30-04	63.7	2.18	TPB-10-70-04	64.2	2.71
TPB-15-30-02	51.7	2.73	TPB-15-70-02	52.6	3.25
TPB-15-30-03	56.1	2.72	TPB-15-70-03	58.1	3.23
TPB-15-30-04	60.6	2.71	TPB-15-70-04	62.3	3.23

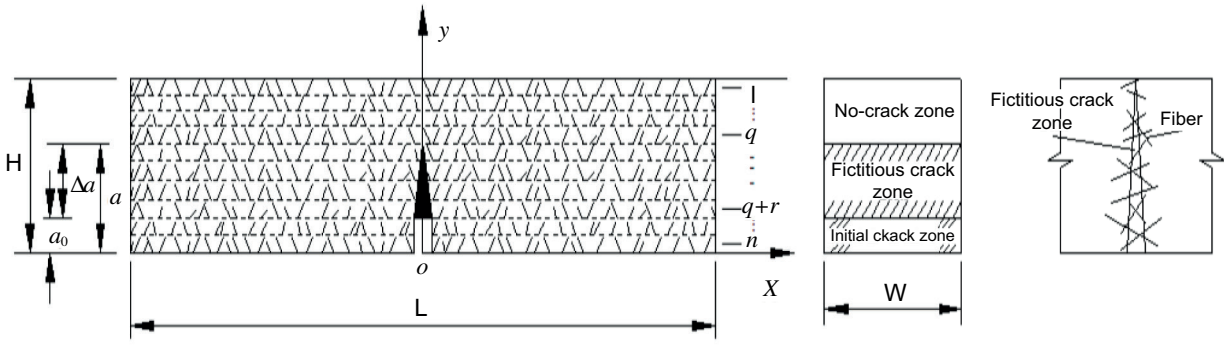

Fig. 2. Layered shear-lag model based on fictitious cracks.

(1) The model of shear-lag analysis

To study the stress redistribution during cracks propagation, a layered shear-lag model was established in **figure 2**.

Assume that the ultimate tensile strength of concrete is f_t, the thickness and height of the TPB concrete beam specimen are t and h, respectively, and the initial length of the crack is a_0. The sample was divided into n sublayers along the height of the beam, where the number of sublayers in the no-crack, fictitious crack, and initial crack zones are q, r, and n-q-r layers, respectively, and the standard height of each sublayer was d ($d = h/n$). For the convenience of calculation, variation layers were set in the first layer of the no-crack zone, the $q + r$ layer of the fictitious crack zone, and the n layer of the initial crack zone, with heights of d_1, d_2, and d_3, respectively. Thus, the initial length (a_0) of the crack can be represented by the fracture of the n-q-r sublayers at $x = 0$. Assuming that each sublayer has only normal stress on the section perpendicular to the y-direction and that the upper and lower surfaces have interlayer shear stress and shear stress caused by the bending deformation of the TPB beam section, the displacement u_i (=1, 2, …, n) of each sublayer should only be a function of the x-direction (the forward direction along the x-axis is the positive direction of the displacement). Take the micro-segment of the ith sublayer with length dx, and its force is shown in **figure 3a**. P_i is the tensile force of the ith sublayer along the x-axis, $\tau_{i-1}(x)$ and τ_i (x) are the shear stress between the upper and lower layers, respectively; $\tau_{rc}(x)$ and $\tau_{rc'}(x)$ are the shear stress caused by the bending deformation of the TPB beam segment, respectively, and $\tau_{I-1}(x)$ and $\tau_I(x)$ are the total shear stress of the upper and lower layers, respectively.

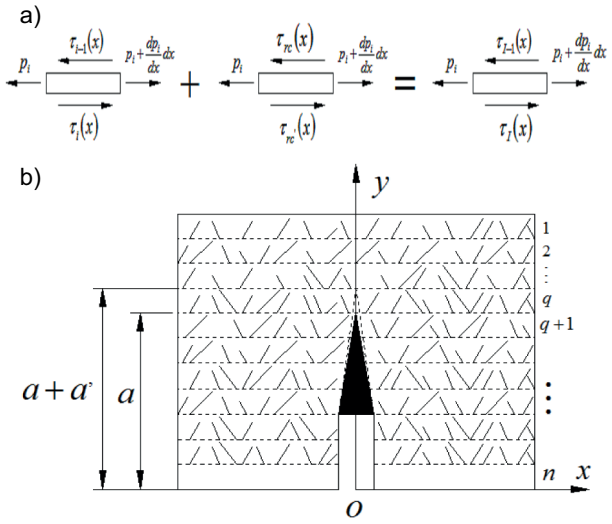

Fig. 3. The fictitious crack analysis model, a) Force diagram of the micro-segment of the ith sublayer; b) Layered shear-lag model based on the expansion of fictitious cracks.

To simplify the calculation, it is assumed that the stress-strain relationship of concrete is linear, therefore,

$$\left.\begin{aligned} p_i(x) &= E_{RSC} A \frac{du_i}{dx} \\ \tau_I(x) &= \frac{G_{RSC}}{d}\left(u_{i+1} - u_i\right), i = 1, 2, \cdots, n \end{aligned}\right\} \quad (1)$$

Where E_{RSC} and G_{RSC} are the elastic modulus and shear modulus of recycled SFRC, respectively. $E_{RSC} = \eta_\theta \eta_b \eta_l E_f \rho_f + E_m (1 - \rho_f)$. If the equivalent fracture toughness of SFRC is calculated, the elastic modulus E_{SC} and shear modulus G_{SC} of SFRC are used. $A = td$ is the cross-sectional area of sublayers. Thus,

the shear hysteresis equilibrium equations of all sublayer microsegments can be listed as

$$\begin{cases}
E_{RSC}A_1\dfrac{d^2u_1}{dx^2}+\dfrac{G_{RSC}t}{d_1}(u_2-u_1)=0\\
E_{RSC}A\dfrac{d^2u_2}{dx^2}+\dfrac{2G_{RSC}t}{d_1+d}(u_1-u_2)+\dfrac{G_{RSC}t}{d}(u_3-u_2)=0\\
E_{RSC}A\dfrac{d^2u_i}{dx^2}+\dfrac{G_{RSC}t}{d}(u_{i+1}-2u_i+u_{i+1})=0,\ i=3,4,\cdots,q+r-2\\
E_{RSC}A\dfrac{d^2u_{q+r-1}}{dx^2}+\dfrac{2G_{RSC}t}{d_2+d}(u_{q+r}-u_{q+r-1})+\dfrac{G_{RSC}t}{d}(u_{q+r-2}-u_{q+r-1})=0\\
E_{RSC}A_2\dfrac{d^2u_{q+r}}{dx^2}+\dfrac{2G_{RSC}t}{d_2+d}(u_{q+r-1}-2u_{q+r}+u_{q+r+1})=0\\
E_{RSC}A\dfrac{d^2u_{q+r+1}}{dx^2}+\dfrac{2G_{RSC}t}{d_2+d}(u_{q+r}-u_{q+r+1})+\dfrac{G_{RSC}t}{d}(u_{q+r+2}-u_{q+r+1})=0\\
E_{RSC}A\dfrac{d^2u_k}{dx^2}+\dfrac{G_{RSC}t}{d}(u_{k+1}-2u_k+u_{k-1})=0,\ k=q+r+2,q+r+3,\cdots,n-2\\
E_{RSC}A\dfrac{d^2u_{n-1}}{dx^2}+\dfrac{2G_{RSC}t}{d_3+d}(u_n-u_{n-1})+\dfrac{G_{RSC}t}{d}(u_{n-2}-u_{n-1})=0\\
E_{RSC}A_3\dfrac{d^2u_n}{dx^2}+\dfrac{2G_{RSC}t}{d_3+d}(u_n-u_{n-1})=0
\end{cases}\tag{2}$$

(2) Determination of equivalent fracture toughness

According to the methods of classical fracture mechanics, the strain energy released during cracks propagation can be obtained by calculating the work required for cracks closure and recovery. The transverse cracks of bending concrete beam belongs to I type crack, its strain energy release rate, i.e., the decrease value of strain energy of the system with cracks propagation unit length is

$$G_I=\lim_{a'\to 0}\frac{1}{a'}\int_0^{a'}\sigma_x\Delta u\,da \tag{3}$$

The finite sublayer model is used to simulate cracks propagation in **figure 3b**. Assuming that the length(a') of cracks propagation is the height (d) of standard sublayer, and the normal stress of the q-layer at $x = 0$ in the nonfracture zone is $\sigma_q(0)$, Equation (3) can be written as

$$G_I=2\sigma_q(0)u_q(0)=2h\sigma_0^{\,2}\cdot\left(E_{RSC}G_{RSC}\right)^{-1/2}\frac{dU_q}{d\xi}(0)U_q(0) \tag{4}$$

According to linear elastic fracture mechanics, under plane strain condition

$$\sigma_0=\frac{M}{W}=\frac{6M}{th^2},\quad G_{IC}=\frac{\left(1-\nu^2\right)}{E}\cdot K_{IC}^2 \tag{5}$$

In this way, the analytical expression of equivalent fracture toughness of concrete beams can be determined by using Equations (4) and (5) as

$$\tilde{K}_{Ic}=6\sqrt{2}M\cdot t^{-1}\cdot h^{-3/2}\left(1-\nu^2\right)^{-1/2}\cdot\left[\frac{dU_q}{d\xi}(0)U_q(0)\right]^{1/2}E_{RSC}^{\ 1/4}G_{RSC}^{\ -1/4} \tag{6}$$

Failure phenomenon of TPB beam specimens

Figure 4 and **figure 5** show the fracture phenomenon and process of the plain concrete beam (Chbani et al. 2019), ordinary SFRC beam, and recycled SFRC beam, respectively. The test process and the load and corresponding velocity diagrams of the cracking process of concrete beams show that the cracks appear faster in the plain concrete TPB beam specimen after loading. Visible cracks appear at the top of the prefabricated incision, which rapidly expand to the loading point at the upper end of the TPB beam, and the entire cracking process shows obvious acceleration. When the fracturing load is reached, the bearing capacity is rapidly lost, and the TPB beam specimen is split in half. The cracking time of the concrete beam is delayed after adding ordinary steel fibers, and the cracking speed of the concrete beam increases slowly in the fracture failure

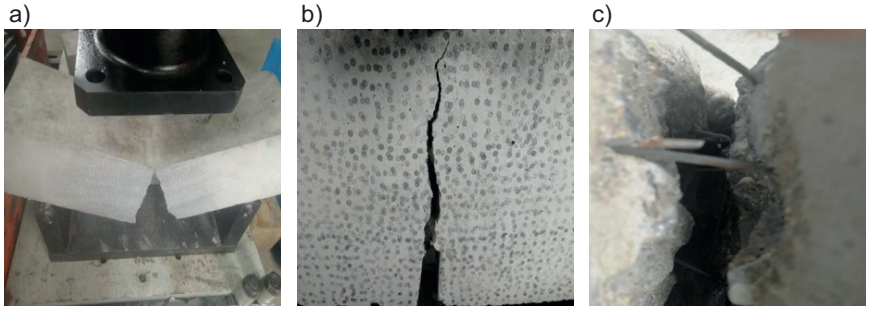

Fig. 4. Fracture phenomenon of TPB beam specimens, a) The fracture of plain concrete; b) The fracture of ordinary steel fiber-reinforced concrete; c) The detail view of fracture of recycled steel fiber-reinforced concrete.

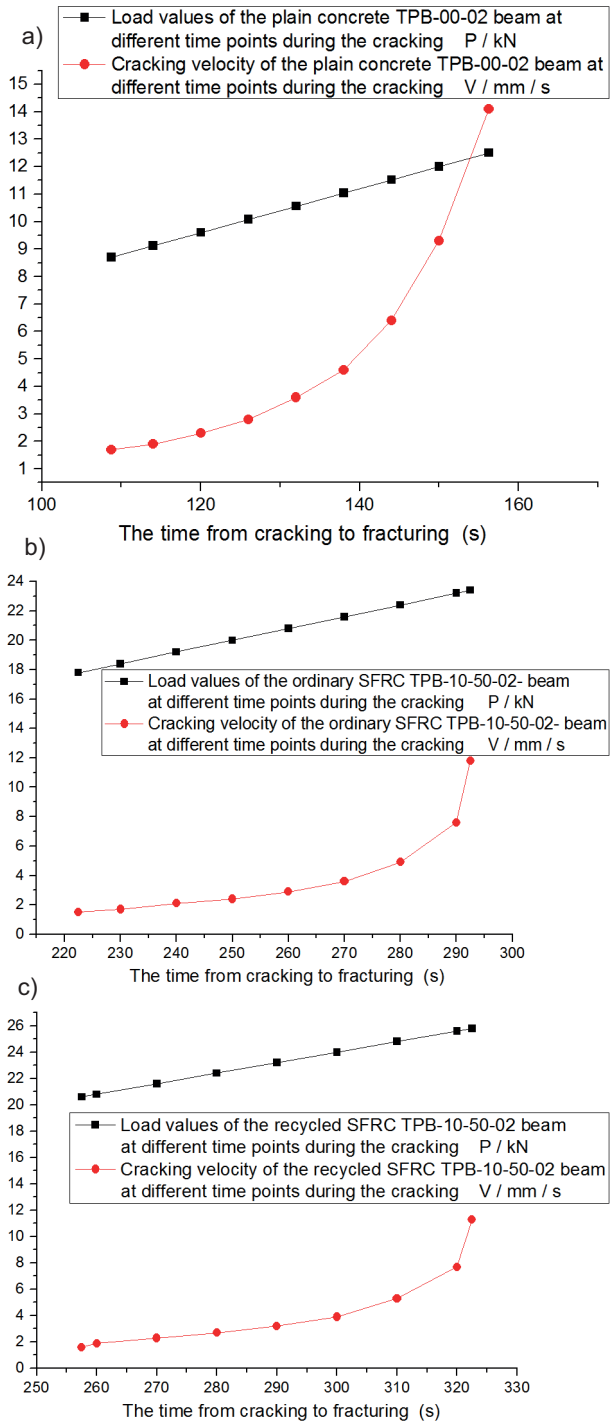

Fig. 5. Fracture process of TPB beam specimens, a) The load and corresponding velocity during the cracking process of plain concrete beam; b) The load and the cracking process of ordinary SFRC beam; c) The load and the cracking process of recycled SFRC beam.

process. This is because the addition of steel fibers can increase the specific surface area of the fracture so that the fracture process needs more energy. The formation of the microcrack zone was blocked by the plastic deformation of steel fibers, and the speed of cracks initiation and propagation is obviously reduced. During the cracking process, the sound of continuous breaking of some ordinary fibers can be heard slightly. After reaching the fracturing load, the steel fiber-reinforced concrete beam gradually lost its bearing capacity. When the recycled steel fibers were added, the cracking speed of the concrete beam in the entire process was slower than that of the ordinary steel fiber-reinforced concrete beam, and the cracking time point was delayed. During the cracking process, the sound of continuous breaking of some recycled steel fibers can be heard. Most specimens remained in a state of cracked and unbroken, and there were still some recycled steel fibers connected at the prefabricated crack section.

Because the internal composition of concrete is nonuniform, the distribution position of coarse and fine aggregates and cement is random. When the cracks started to expand upward from the prefabricated incision tip, the weakest places were always selected for the extension. Therefore, the primary cracks inside the concrete were the first to expand. As the load continued to increase, the fine cracks were connected to form a larger crack propagation that does not rise in a straight line. Moreover, because of the recycled steel fibers, the expansion direction of cracks constantly changed, presenting a multipoint cracking state. As the cracks expand, fine aggregate and cement will be removed from the joint. When the cracks meet the coarse aggregate, they might change the original expansion path (bypass the joint surface) or break the recycled steel fibers and pull out the coarse aggregate. Then, the cracks continued to expand and quickly passed through the specimen, and the cracks changed from numerous cracks to large macroscopic cracks, until the TPB beam specimen finally broke.

Through observation, the damage phenomenon of stones at the sections of three TPB beams was obvious. When the TPB beam specimens with recycled steel fibers reached the cracking load, the recycled steel fibers perpendicular to the cracks in the concrete can continue to bear and transfer more stress, they can delay the cracking of concrete matrix better than ordinary steel fibers. There is obvious stratification at the fracture surface above prefabricated incision of recycled SFRC. After the load were applied, the recycled steel fibers in different layers will bear different stress lengths and tensile forces at the same stress moment. When the steel fibers in the lower layer at the fracture surface loses its bearing effect, the steel

fibers in the upper layer can continue to bear the stress transfer effect. **Figure 6** shows the comparison of cracking and fracturing loads of three concrete beams with different relative incision depths. It can be seen that from the plain concrete beam to the ordinary SFRC beam, and then to the recycled SFRC beam, the cracking and fracturing loads gradually increase.

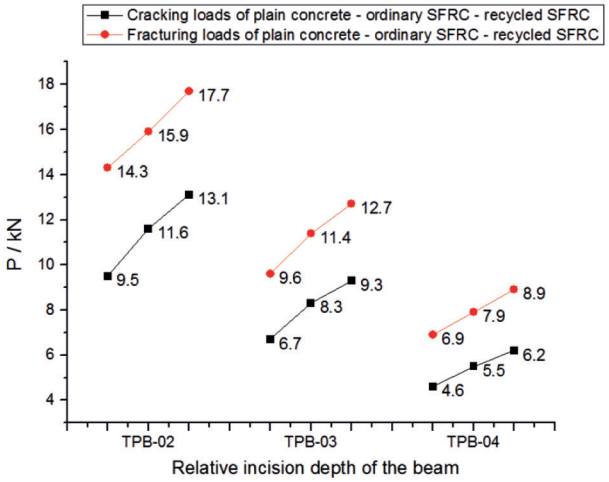

Fig. 6. Comparison of cracking and fracturing load values of three kinds of concrete beams.

Influence of fiber contents on load values and equivalent fracture toughness

Figure 7 shows the variation trends of load values and equivalent fracture toughness of TPB concrete specimens with different contents of recycled steel fibers. The cracking load, fracturing load, and equivalent fracture toughness increase as the content of recycled steel fibers increases. Taking the concrete specimen with length-diameter ratio of 30 and relative incision depth of 0.2 as an example: after the 0.5% ordinary steel fibers are added, the cracking load of the TPB beam specimen increases from 9.5 kN to 11.6 kN. The fracturing load increases from 14.3 kN to 15.9 kN, and the equivalent fracture toughness increases from 1.20 $MPa \cdot m^{1/2}$ to 1.38 $MPa \cdot m^{1/2}$. However, when the content of added recycled steel fibers reaches 0.5%, the cracking load rises to 13.1 kN, the fracturing load increases to 17.7 kN, and the equivalent fracture toughness increases to 1.54 $MPa \cdot m^{1/2}$. Therefore, the recycled steel fibers can delay crack initiation of the specimen better than ordinary steel fibers. When the recycled steel fiber content is 0.5%-1.5%, the cracking load of the concrete specimen increases by 5.1 kN, the fracturing

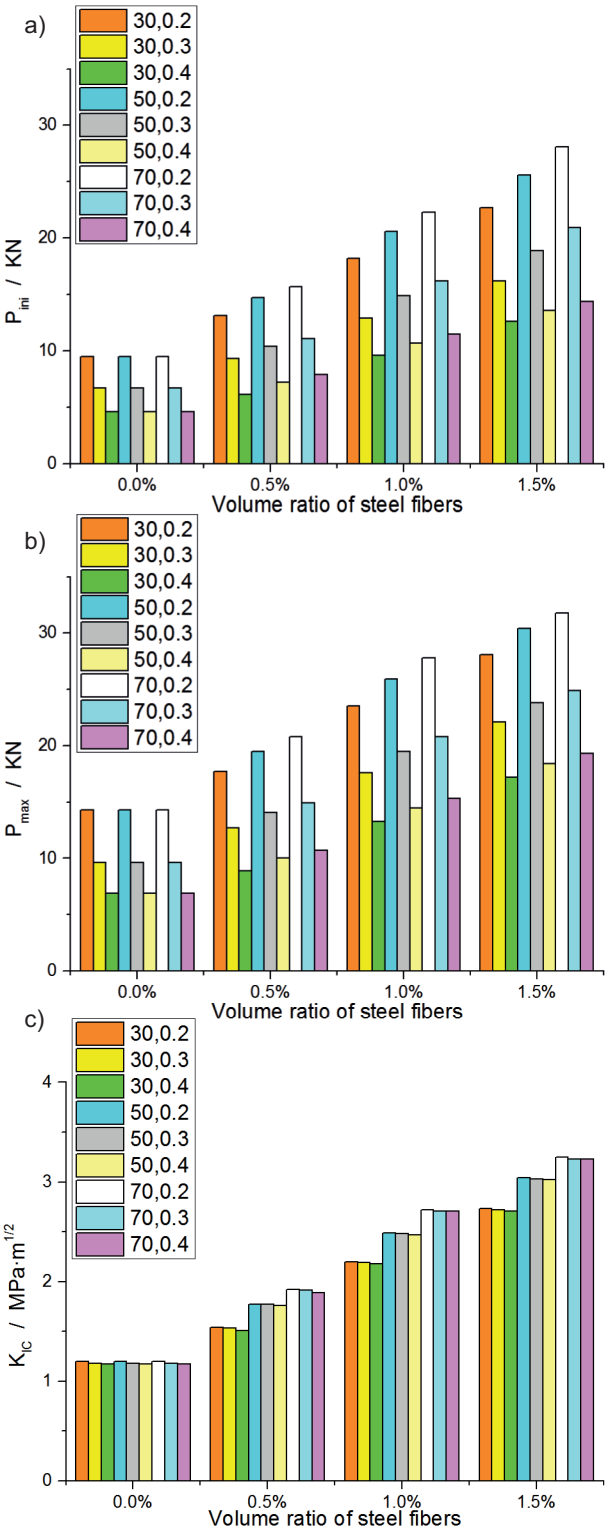

Fig. 7. Influence of fiber contents on load values and equivalent fracture toughness, a) Relationship between cracking loads and fiber contents; b) Relationship between fracturing loads and fiber contents; c) Relationship between equivalent fracture toughness and fiber contents.

load increases by 5.8 kN, and the equivalent fracture toughness increases by 0.66 $MPa \cdot m^{1/2}$. When the volume content of recycled steel fibers continues to increase by 0.5%, the cracking load of the concrete specimen increases by 4.5 kN, the fracturing load only increases by 4.6 kN, and the equivalent fracture toughness increases by 0.53 $MPa \cdot m^{1/2}$. Other steel fiber-reinforced concrete specimens present a similar growth pattern. It can be seen that the load characteristic values and equivalent fracture toughness of concrete beams increase with the increases of volume content of recycled steel fibers, and when the fiber content is from 0.0% to 1.0%, the increased amplitude of load characteristic values and equivalent fracture toughness of concrete beams gradually increases, when the fiber content is from 0.5% to 1.0%, the increased amplitude of load characteristic values and equivalent fracture toughness of concrete beams reaches the maximum, and when the fiber content is from 1.0% to 1.5%, the increased amplitude of load characteristic values and equivalent fracture toughness of concrete beams decreases. This indicates that when the content of recycled steel fibers is 1.0%, the network structure at the prefabricated crack tip reaches a certain degree of compactness and is in the optimal fiber reinforcement interval. When the fiber content continues to increase, the hindering effect of the network structure becomes less obvious, and the increasing effect of cracking loads, fracturing loads and equivalent fracture toughness of concrete beams is weakened.

Influence of fiber length-diameter ratios on load values and equivalent fracture toughness

Figure 8 shows the variations of load values and equivalent fracture toughness of recycled steel

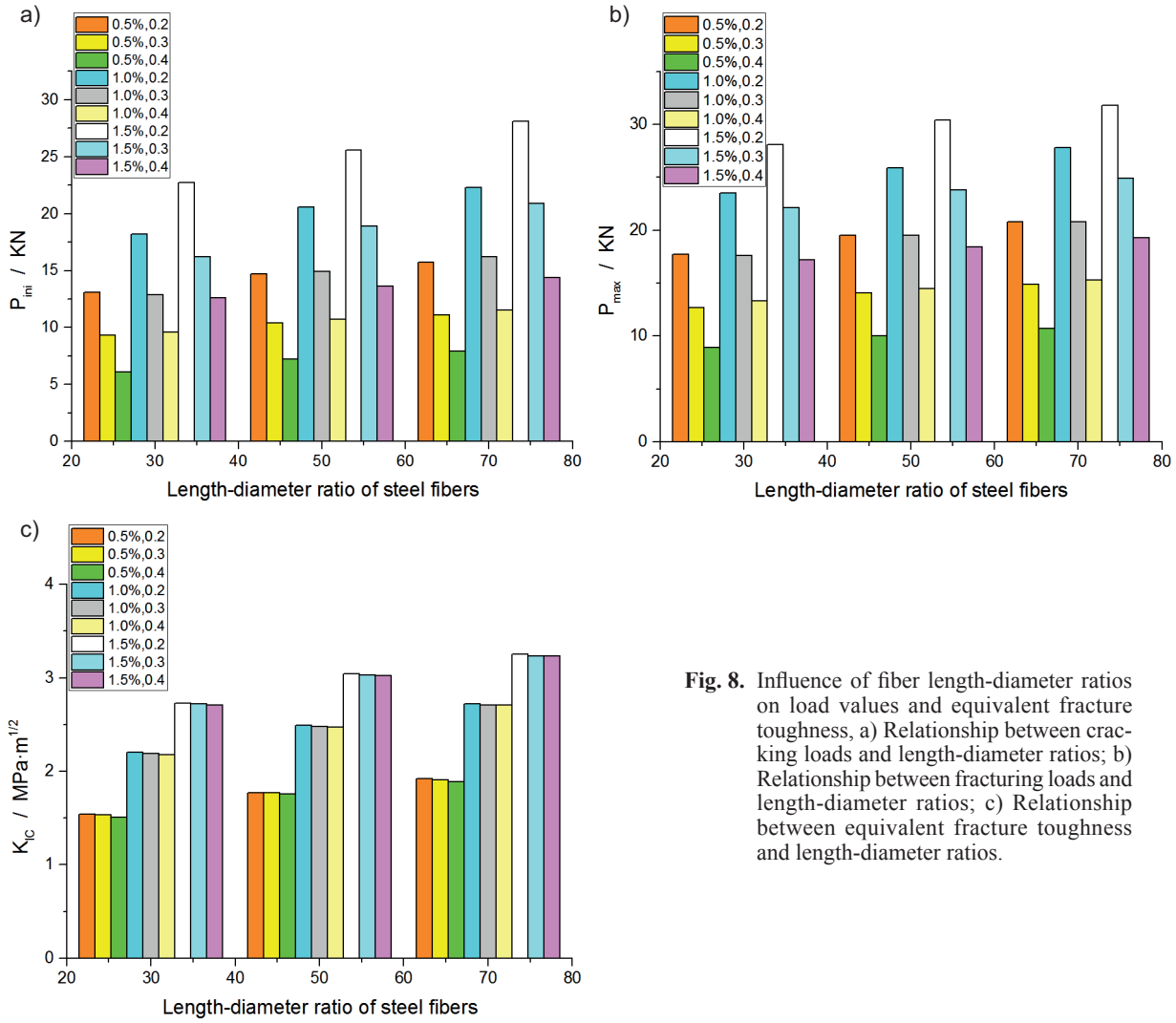

Fig. 8. Influence of fiber length-diameter ratios on load values and equivalent fracture toughness, a) Relationship between cracking loads and length-diameter ratios; b) Relationship between fracturing loads and length-diameter ratios; c) Relationship between equivalent fracture toughness and length-diameter ratios.

fiber-reinforced TPB beam specimens under different fiber length-diameter ratios. Taking the specimen with fiber content of 0.5% and relative incision depth of 0.3 as an example: when the ordinary steel fibers with length-diameter ratio of 30 are added, the cracking load increases from 6.7 kN to 8.3 kN, the fracturing load increases from 9.6 kN to 11.4 kN, and the equivalent fracture toughness increases from 1.18 $MPa \cdot m^{1/2}$ to 1.36 $MPa \cdot m^{1/2}$. When recycled steel fibers are added, the cracking load are, respectively, 9.3 kN (length-diameter ratio is 30), 10.4 kN (length-diameter ratio is 50), and 11.1 kN (length-diameter ratio is 70), the cracking load increases by 1.1 kN and 0.7 kN, respectively. The fracturing loads are 12.7 kN (length-diameter ratio is 30), 14.1 kN (length-diameter ratio is 50), and 14.9 kN (length-diameter ratio is 70), respectively, which increases by 1.4 kN and 0.8 kN, respectively. The equivalent fracture toughness is 1.53 $MPa \cdot m^{1/2}$ (length-diameter ratio is 30), 1.77 $MPa \cdot m^{1/2}$ (length-diameter ratio is 50), and 1.91 $MPa \cdot m^{1/2}$ (length-diameter ratio is 70), respectively, which increases by 0.24 $MPa \cdot m^{1/2}$ and 0.14 $MPa \cdot m^{1/2}$, respectively. Simultaneously, by comparing and analyzing the load values of other specimens, we found that the recycled steel fibers can delay the crack initiation of specimens better than ordinary steel fibers. When the length-diameter ratio of the recycled steel fibers changes from 30 to 50 to 70, the load values and the equivalent fracture toughness of concrete beams gradually increase. When the length-diameter ratio of recycled steel fibers changes from 30 to 50, the load values and the equivalent fracture toughness of concrete beams increase relatively large. When the length-diameter ratio of recycled steel fibers changes from 50 to 70, the load values and the equivalent fracture toughness of concrete beams increase relatively small. That is because when the TPB beam specimen is destroyed, the crack expands from a microscopic crack to a macroscopic crack. During cracks propagation, some recycled steel fibers with relatively small length-diameter ratio will be pulled out, whereas the recycled steel fibers with length-diameter ratio of 50 and 70 can still play the bridging role, that is, compared with the specimens with length-diameter ratio of 30, the ductility and toughness of specimens with length-diameter ratio of 50 and 70 are somewhat improved.

Influence of relative incision depths on load values and equivalent fracture toughness

Figure 9 shows the variations of load values and equivalent fracture toughness of recycled steel fiber-reinforced TPB beam specimens with different relative incision depths. For the concrete specimen with volume content of 1.0% and length-diameter ratio of 50, the cracking and fracturing loads of a plain concrete beam with relative incision depth of 0.2 are 9.5 kN and 14.3 kN, respectively, and the equivalent fracture toughness is 1.20 $MPa \cdot m^{1/2}$. When the relative incision depth is 0.2, the cracking and fracturing loads of an ordinary SFRC beam are 17.9 kN and 23.4 kN, respectively, and the equivalent fracture toughness is 2.23 $MPa \cdot m^{1/2}$. However, when the relative incision depth is 0.2, the cracking and fracturing loads of the recycled SFRC beam are 20.6 kN and 25.9 kN, respectively, and the equivalent fracture toughness is 2.49 $MPa \cdot m^{1/2}$. When the relative incision depth of the recycled SFRC beam changes from 0.2 to 0.3, the cracking and fracturing loads decrease by 5.7 kN and 6.4 kN, respectively, and the equivalent fracture toughness only decreases by 0.01 $MPa \cdot m^{1/2}$. When the relative incision depth of the recycled SFRC beam changes from 0.3 to 0.4, the cracking and fracturing loads decrease by 4.2 kN and 5.0 kN, respectively, and the equivalent fracture toughness also decreases by only 0.01 $MPa \cdot m^{1/2}$. Analysis of the figures shows that recycled steel fibers have a better effect on delaying crack initiation of specimens than ordinary steel fibers. The cracking and fracturing loads of TPB beam specimens decrease as the relative incision depth increases. When the relative incision depth changes from 0.2 to 0.3, the load values of concrete beams decrease relatively large, and when the relative incision depth changes from 0.3 to 0.4, the load values of concrete beams decreases relatively small. Moreover, compared with the cracking load, the decreasing amplitude of the fracturing load is relatively larger. The equivalent fracture toughness of concrete beams almost does not change with the changes in the relative incision depth.

FRACTURE SIMULATION AND RESULTS ANALYSIS OF TPB BEAMS BASED ON EXTENDED FINITE ELEMENT METHOD

The basic theory of extended finite element method

The numerical simulation of recycled SFRC has two theoretical bases: one is based on fracture mechanics (Clerc et al. 2020), the other on damage mechanics (Li and Cui 2020). The traditional cracking calculation technique is strict to the grid division and computation-intensive when the continuous displacement shape function is used to obtain sufficient precision. Therefore, in 1999, Belytschko's research group proposed the extended finite element method

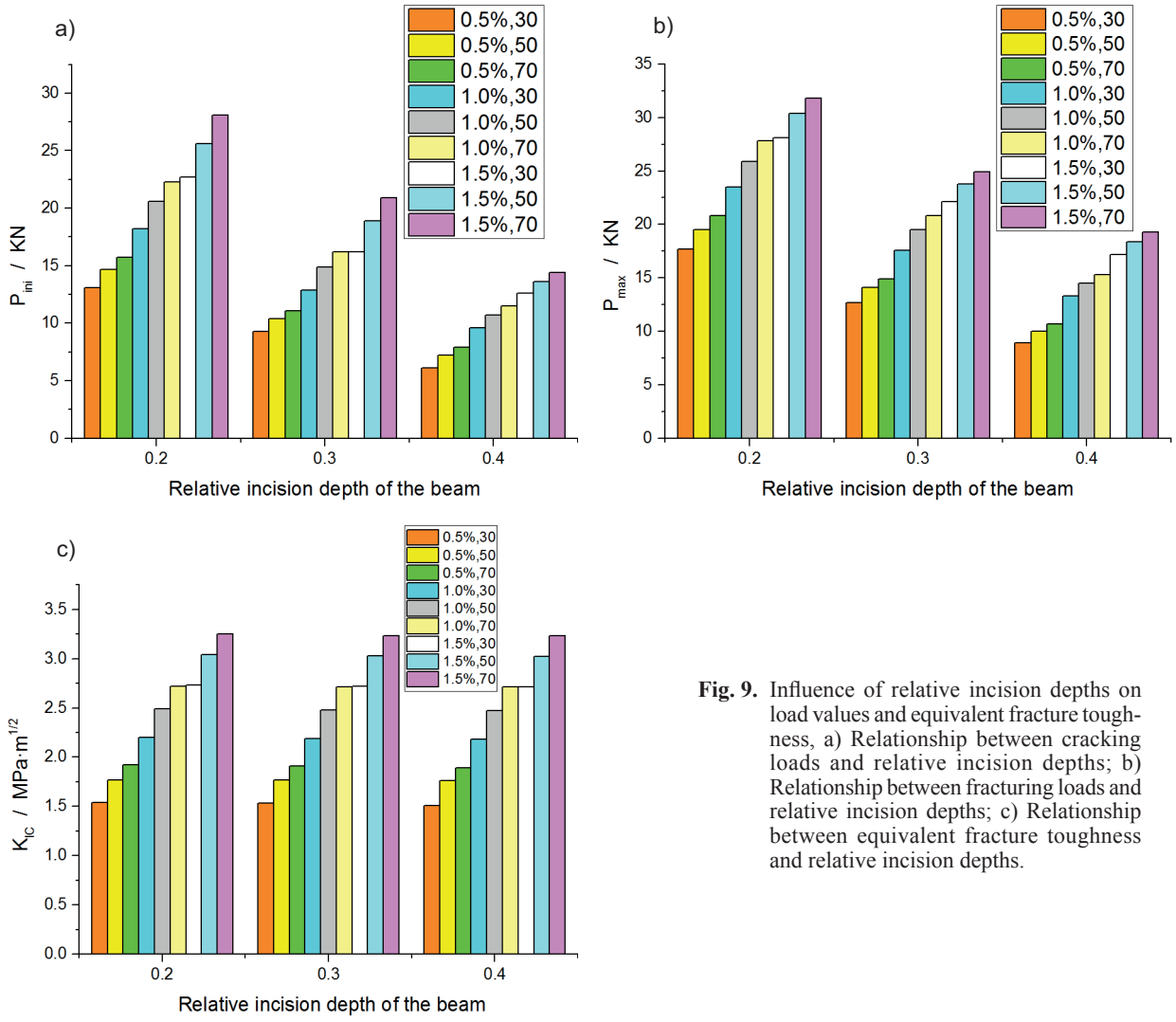

Fig. 9. Influence of relative incision depths on load values and equivalent fracture toughness, a) Relationship between cracking loads and relative incision depths; b) Relationship between fracturing loads and relative incision depths; c) Relationship between equivalent fracture toughness and relative incision depths.

(FEM) (Tang and Chen 2018). This method separates the crack calculation grid from the geometric model and solves the limitation of considering the displacement discontinuity caused by the crack and redividing the grid in the traditional FEM. In the extended FEM, the cracks can crack from the inside of the element, and the shape and direction of cracks does not need to be considered, and the entire process of cracks propagation in the fracture failure behavior can be simulated automatically.

Constitutive relations of concrete

When using ABAQUS finite element software for numerical simulation analysis, it is particularly important to use the constitutive relation of concrete for nonlinear analysis of specimens. According to the previous experience, the plastic damage model of concrete is used for analysis, and the inelastic behavior of the model (continuum damage model of plasticity) is assumed to take the material as the concepts of isotropic elastic damage, isotropic tensile and isotropic compressive plasticity. It is assumed that the yield surface of two main failure mechanisms of concrete materials, tensile cracking and compressive brittle failure, is controlled by the equivalent compression and equivalent tensile plastic strain and the unrelated flow law. According to the constitutive relationship of concrete in Code for Design of Concrete Structures (GB50010-2010), the stress-strain calculation of concrete is as follows, and the constitutive curve of concrete is shown in **figure 10**.

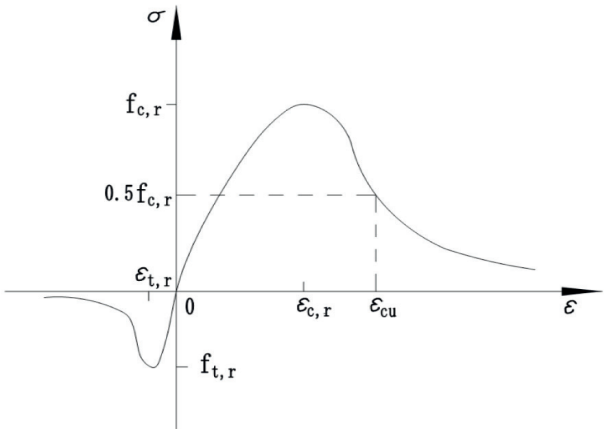

Fig. 10. Uniaxial stress-strain curve of concrete.

The stress-strain curve of concrete under uniaxial compression in **figure 10**, which is calculated according to the following formulas:

$$\sigma = (1-d_c)E_c\varepsilon \tag{1}$$

$$d = 1-\frac{\rho_c n}{n-1+x^n} \qquad x \le 1 \tag{2}$$

$$d = 1-\frac{\rho_c}{\alpha_c(x-1)^2+x} \qquad x > 1 \tag{3}$$

$$\rho_c = \frac{f_{c,r}}{E_c\varepsilon_{c,r}} \tag{4}$$

$$n = \frac{E_c\varepsilon_{c,r}}{E_c\varepsilon_{c,r}-f_{c,r}} \tag{5}$$

$$x = \frac{\varepsilon}{\varepsilon_{c,r}} \tag{6}$$

Where: α_c is the parameter value of the stress-strain curve descending section of concrete under uniaxial compression; $f_{c,r}$ is the representative value of uniaxial compressive strength of concrete, and f_c, f_{ck} or f_{cm} can be taken respectively according to the needs of actual structural analysis; $\varepsilon_{c,r}$ is the peak compressive strain corresponding to the representative value of uniaxial compressive strength of concrete; d is the evolution parameter of uniaxial compression damage of concrete.

The stress-strain curve of concrete under uniaxial tension in **figure 10** can be calculated according to the following formulas:

$$\sigma = (1-d_t)E_c\varepsilon \tag{1}$$

$$d_1 = 1-\rho_t(1.2-0.2x^5) \qquad x \le 1 \tag{2}$$

$$d_1 = 1-\frac{\rho_t}{\alpha_t(x-1)^{1.7}+x} \qquad x > 1 \tag{3}$$

$$x = \frac{\varepsilon}{\varepsilon_{t,r}} \tag{4}$$

$$\rho_t = \frac{f_{t,r}}{E_c\varepsilon_{t,r}} \tag{5}$$

Where, α_t is the parameter value of the stress-strain curve descending section of concrete under uniaxial tension; $f_{t,r}$ is the representative value of uniaxial tensile strength of concrete, and f_t, f_{tk} or f_{tm} can be taken respectively according to the needs of actual structural analysis; $\varepsilon_{t,r}$ is the peak tensile strain corresponding to the representative value of uniaxial tensile strength of concrete; d_1 is the evolution parameter of uniaxial tensile damage of concrete.

Constitutive relations of recycled steel fibers

Compared with the brittle material (concrete), the constitutive relationship of steel wire recycled from industrial waste tires is not complicated. The nature of recycled steel fibers belongs to steel, and some classical constitutive relations proposed by previous researchers can be adopted and used. So the bilinear follow-up strengthening model is directly adopted in this paper. Therefore, the stress-strain relationship of recycled steel fibers is shown in **figure 11**. The initial elastic modulus is E_0, and the plastic modulus (E_1) entering the plastic stage after yielding is 1.0% of the initial elastic modulus, namely:

$$E_1 = 0.01E_0$$

The building of the model

Finite element numerical models of recycled steel fiber-reinforced TPB beam specimens were established in this study. The size of the beam specimen in the model is L × W × H = 550 mm × 150 mm × 150 mm. The middle span is 400 mm, and the width of the reserved seam at the bottom is 20 mm, which is consistent with the TPB beam in the test. During the simulation, the recycled steel fibers are generated by Python script and distributed evenly in the concrete module as in the test (Ren and Li 2013).

(1) Assignments of material properties

According to the FEM analysis, the material properties were set as elastic-plastic materials

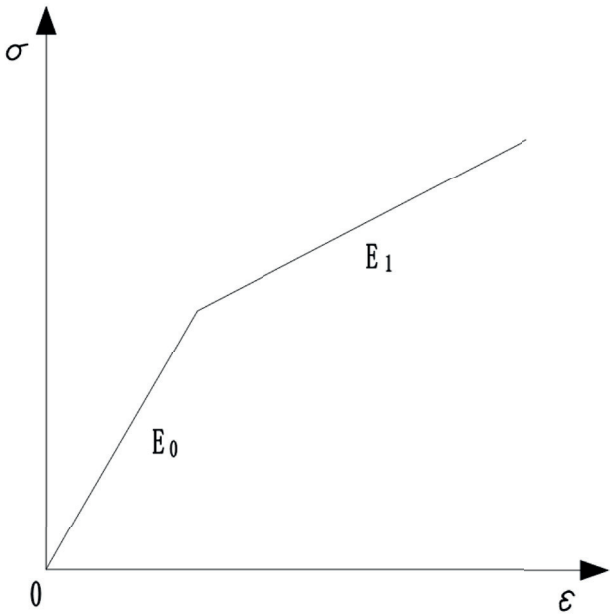

Fig. 11. Stress-strain relationship of recycled steel fibers.

according to the research results and experiments of domestic and foreign experts and scholars, the relevant parameters of recycled SFRC were selected, as shown in **table III**.

(2) Boundary conditions and loading

The simple support constraints were set at 200 mm to the left and right of the prefabricated incision at the bottom of the TPB beam. The right support constrains displacement in the X and Y directions, and the left support constrains displacement in the y direction. The loading mode of the simulation and test is consistent, which adopts continuous loading.

(3) The division of the grid

The grid division is critical in the establishment of geometric model. The grid division is based on the extended FEM in ABAQUS. The extended FEM does not support adaptive meshes, and the influence of the unit density and types at the seam end on the calculation results is extremely limited. To improve the efficiency, grid subdivision is no longer required at the seam end, and the CPS4R 4 node plane stress unit was used in all unit divisions. **Figure 12** shows the grid division of a TPB beam.

(4) Criterion of destruction

Under the action of the external loads, micro-cracks in the specimen are generated and collected, resulting in macroscopic cracks, and eventually, failure occurs in the maximum principal stress direction. The tensile strength of recycled steel fibers is

TABLE III. PARAMETERS OF EACH COMPONENT OF RECYCLED SFRC.

Component	Density (kg / m^3)	Tensile strength (MPa)	Modulus of elasticity (GPa)	Poisson's ratio	Fracture energy (N / m)
Concrete matrix	2400	1.8	33	0.16	110
Recycled steel fiber	7900	1800	216	0.3	—

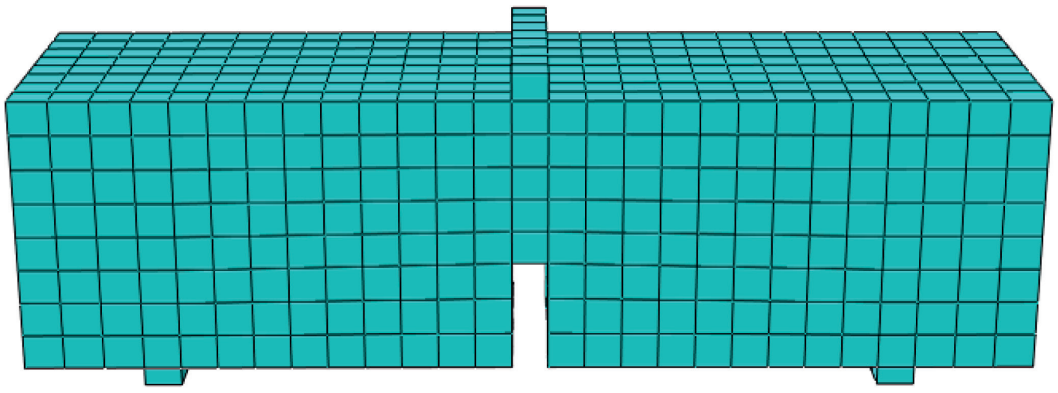

Fig. 12. Grid division diagram of a TPB beam.

much higher than coarse aggregate, fine aggregate and cement. It is assumed that recycled steel fibers are ideal elastic-plastic materials in this model, and the damage of recycled steel fibers is not considered.

In the maximum tensile stress criterion, fracture can occur if the maximum tensile stress (σ_1) reaches the limit value of tensile strength (R_m) of the material. Therefore, the failure condition of TPB beam specimens is $\sigma_1 = R_m$.

Analysis of stress nephograms and cracking situation of three-point bending concrete beams

In practical engineering, SFRC with volume content of 1.0% is more widely used and has many research value. Therefore, the fracture simulation of recycled SFRC with volume content of 1.0% was conducted. The fiber length-diameter ratios and relative incision depths were set in accordance with the standards in the test.

Figures 13 to **15** show that the length-diameter ratio of recycled steel fibers has a significant influence on the final morphology of cracks during the test (Xia et al. 2011). As the length-diameter ratio of recycled steel fibers increases, the cracked area on the upper part of the incision of TPB beam specimens gradually decreases, which is consistent with the test. When the length-diameter ratio of recycled steel fibers is small, the cracks are mostly bypassed from the end of steel fibers, and the recycled steel fibers has little effect on the change of crack paths. As the fiber length-diameter ratio increases, more paths and more energy are needed for cracks propagation. Therefore, as the length-diameter ratio increases, the cracking and fracturing loads of TPB beam specimens will increase.

Figures 13 to **16** show that as the relative incision depth increases, the cracked area on the upper part of the incision of TPB beam specimens gradually increases, and the cracking time gradually becomes shorter. During the entire cracking process, the cracking speed of concrete beams with relative incision depth of 0.3 is higher than that of concrete beams with relative incision depth of 0.2, which is consistent with the test. The cracking speed of concrete beams with relative incision depth of 0.4 is slightly higher than that of concrete beams with relative incision depth of 0.3 in the early stage, and the cracking speed increases for more than 10 seconds in the later stage, which is slightly faster than that of concrete beams in the same period in the test. Furthermore, the bending degree of concrete beams with relative incision depth of 0.3 is the largest before fracture, whereas the bending degree of concrete beams with relative incision depth of 0.3 and 0.4 shows no significant difference during the test. The analysis of the crack strain nephograms of concrete beams with three relative incision depths shows that when the cracks expand, the expansion trajectory is centered on the tip of the prefabricated incision and cracking upward first, and then cracking freely to both sides. Overall, the cracks expansion area is symmetrically distributed to some extent with the prefabricated incision as the center, and there is also obvious stratification at the crack surface of the upper part of the prefabricated incision. These are also consistent with the propagation of cracks in the test, and the validity of the extended FEM simulation of fracture behavior is verified. However, in the experiment, the macroscopic cracks and many microcracks coexisted in the fracture failure process of TPB beams. Instead of simply cracking roughly in straight lines along the prefabricated incision, the cracks had a certain degree of bending in the actual propagation, which was the biggest difference between the simulation and experiment. Furthermore, cracks also appeared in the contact part between the concrete beam and pad in the test, but the cracks were not as obvious as those in the simulation. The simulation in this study mainly involves the propagation of single crack, and there is no further study on the propagation of multiple cracks.

Analysis of stress nephograms of recycled steel fibers

Figure 17 shows the stress nephograms of recycled steel fibers with length-diameter ratio of 50 in the TPB beams with different relative incision depths in the simulation. As can be seen from the figures, as the relative incision depth of the concrete beam gradually increases, the stress borne by recycled steel fibers gradually increases, that is, the recycled steel fibers can play a role in delaying the crack initiation of specimens, and can improve the crack resistance of concrete beams. At the same time, it can be seen that the recycled steel fibers at the upper part of the precast incision bear a relatively large stress, which can also indicate that the existence of recycled steel fibers makes the cracks expansion need to consume more energy, so as to delay the crack initiation of concrete beams. The above are consistent with the test.

Comparative analysis of simulation results and test results

Taking the Test Procedure for Fracture of Hydraulic Concrete (DLT5332-2005) as the standard, the unstable fracture toughness (K^S_{IC}) of the matrix is calculated by using

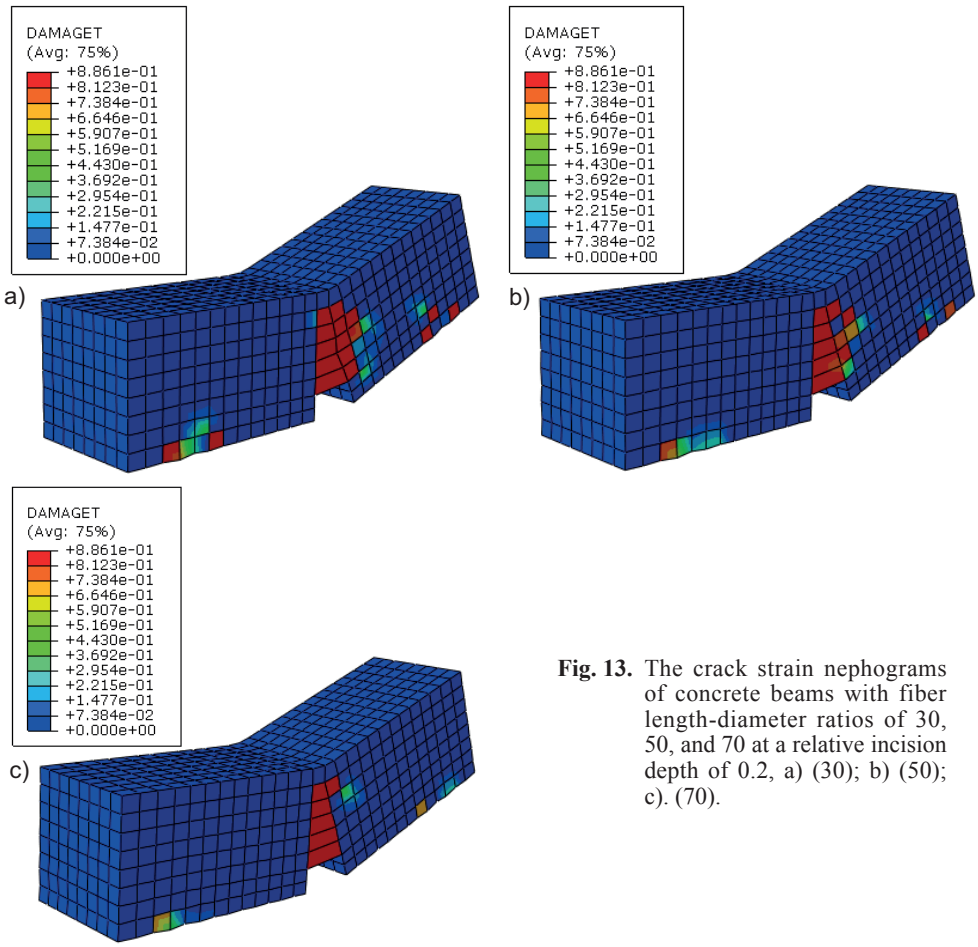

Fig. 13. The crack strain nephograms of concrete beams with fiber length-diameter ratios of 30, 50, and 70 at a relative incision depth of 0.2, a) (30); b) (50); c). (70).

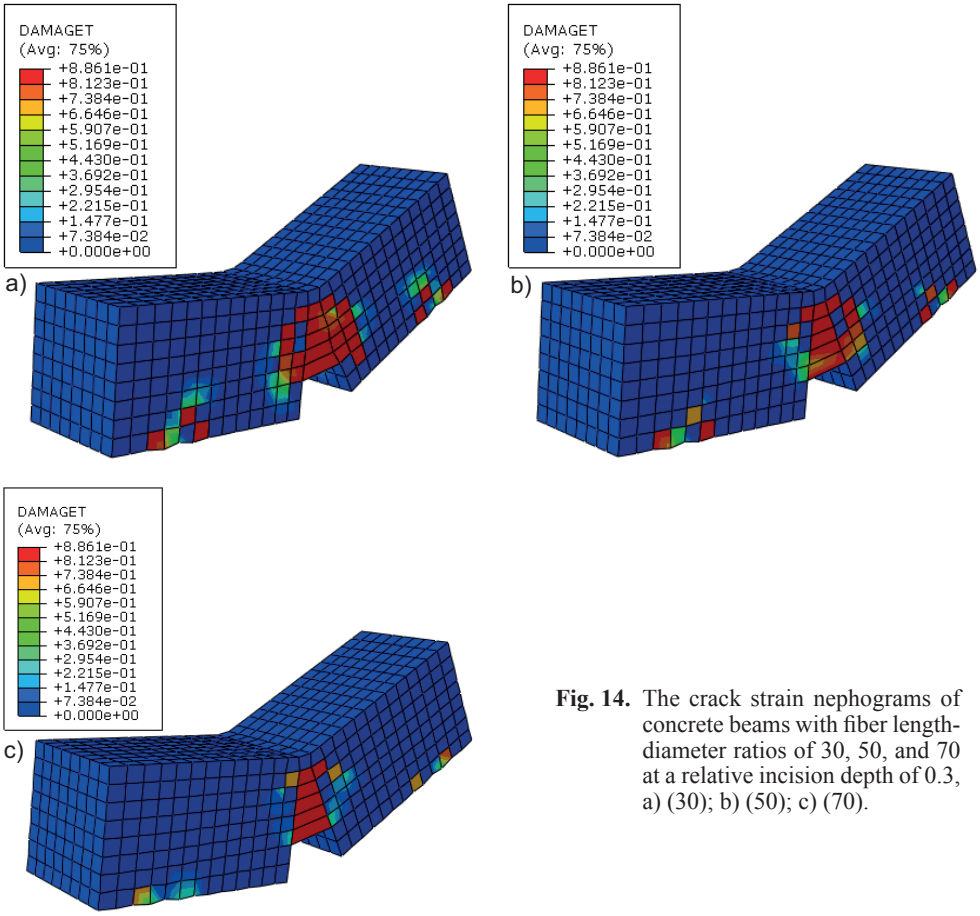

Fig. 14. The crack strain nephograms of concrete beams with fiber length-diameter ratios of 30, 50, and 70 at a relative incision depth of 0.3, a) (30); b) (50); c) (70).

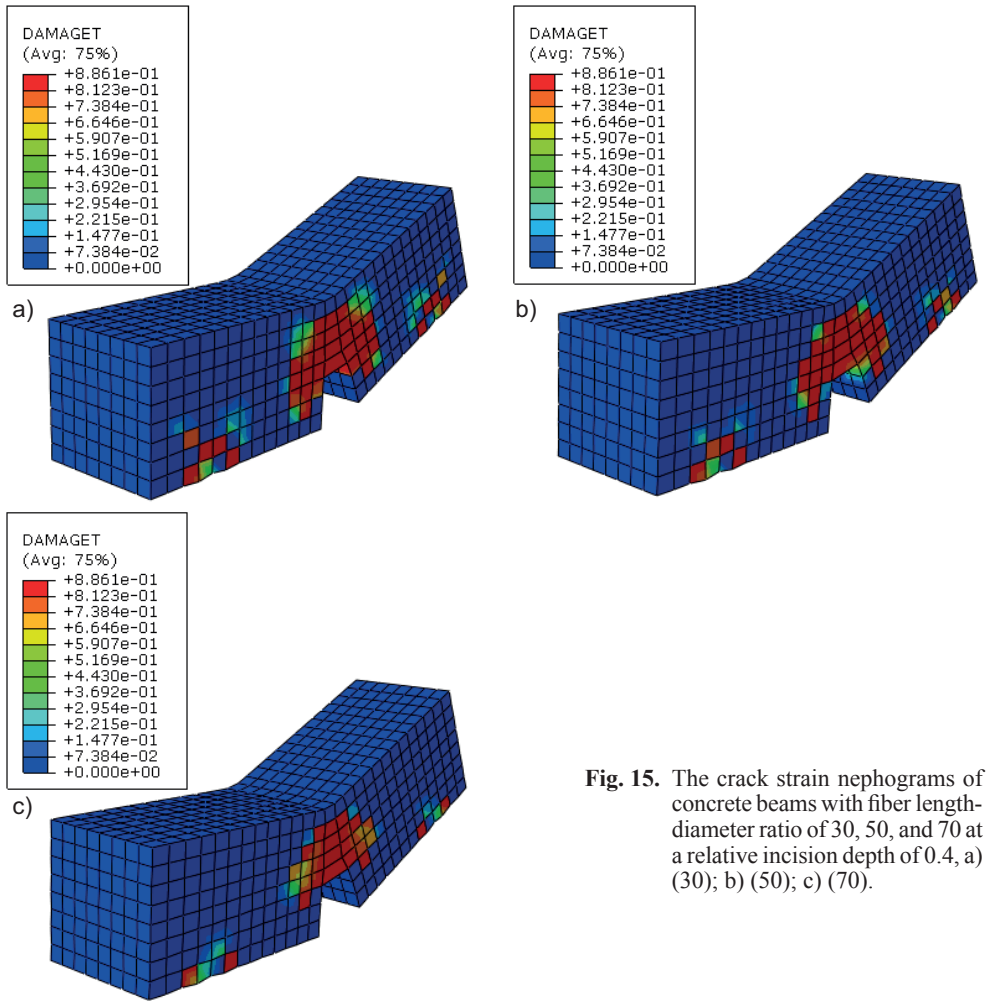

Fig. 15. The crack strain nephograms of concrete beams with fiber length-diameter ratio of 30, 50, and 70 at a relative incision depth of 0.4, a) (30); b) (50); c) (70).

$$K_{IC}^{S} = \frac{1.5\left(F_S + \frac{mg}{2}\times 10^{-2}\right)\times 10^{-3} S\cdot\sqrt{a_c}}{th^2} f(\alpha),$$

$$f(\alpha) = \frac{1.99 - \alpha(1-\alpha)\times\left(2.15 - 3.93\alpha + 2.7\alpha^2\right)}{(1+2\alpha)\times(1-\alpha)^{3/2}},$$

$$\alpha = \frac{a_c}{h}$$

Where F_S is the unstable load (kN) and a_c is the length of the crack (mm).

From **table IV**, the following conclusions can be drawn:

(1) The above data of recycled SFRC beams with different fiber length-diameter ratios show that the relative error between the load characteristic values and unstable fracture toughness in the test and those of in the simulation are within the allowable range. The analysis reveals that the results in the simulation agree with the conclusions obtained in the test, that is, as the fiber length-diameter ratio increases, the cracking loads, fracturing loads, and unstable fracture toughness of TPB beam specimens of the same size increase, that is, the fracture performance increases.

(2) The error between the load characteristic values and unstable fracture toughness of concrete beams with different relative incision depths in the simulation and those of in the test are within the allowable range. From the simulation, we can see that with the relative incision depth increases, the cracking and fracturing loads of TPB beam specimens decrease, and the unstable fracture toughness has little change with the changes in the relative incision depth, which

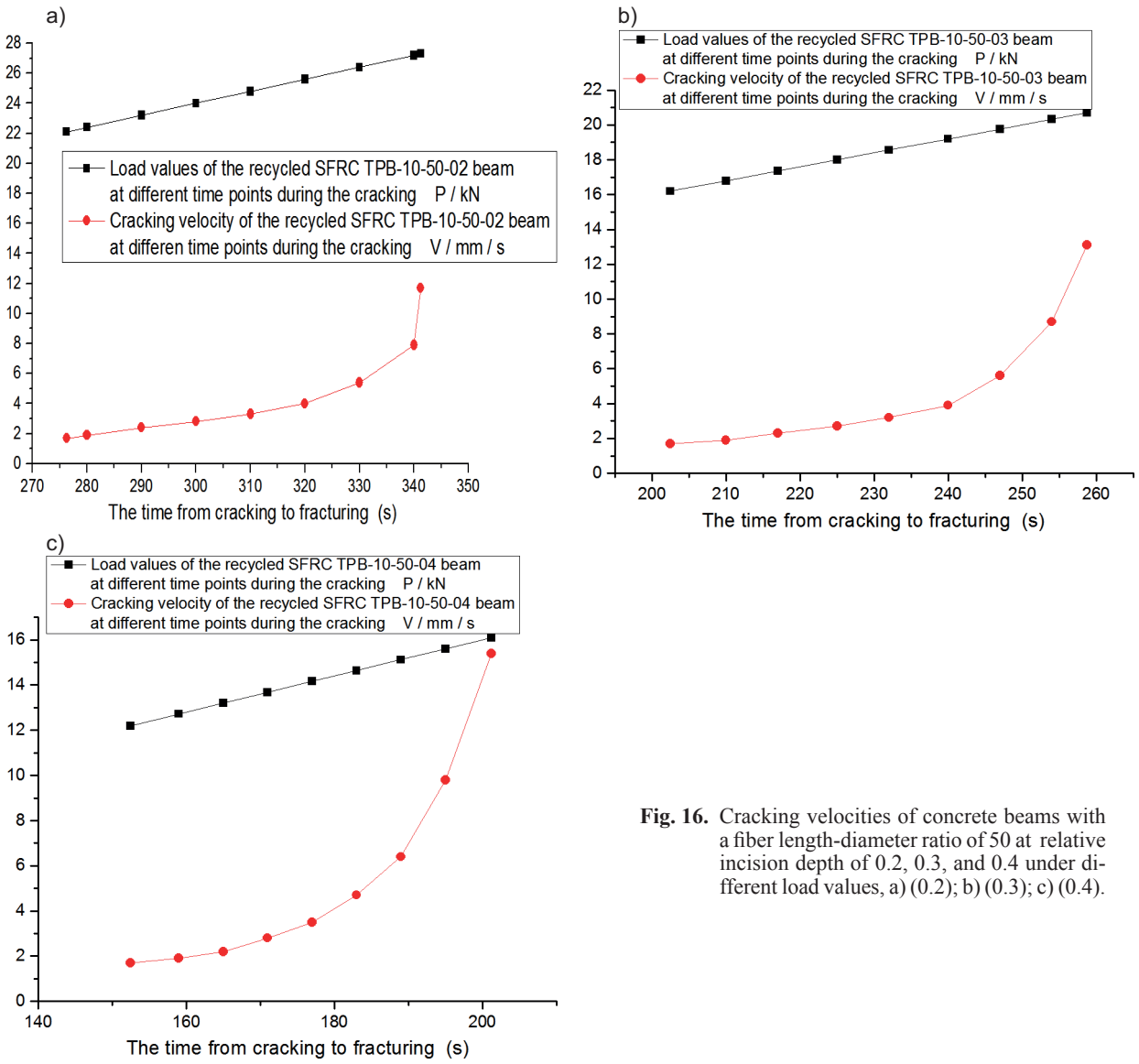

Fig. 16. Cracking velocities of concrete beams with a fiber length-diameter ratio of 50 at relative incision depth of 0.2, 0.3, and 0.4 under different load values, a) (0.2); b) (0.3); c) (0.4).

are also consistent with the conclusions in the test.

CONCLUSIONS AND PROSPECTS

Conclusions

In this study, the fracture performance of recycled SFRC was taken as the principal research direction. The research results and cause analysis of the fracture performance of several types of concrete beams were obtained based on DIC technology, and the following conclusions are drawn:

(1) The addition of steel fibers significantly improves the crack resistance of concrete beams, and the effect of recycled steel fibers is better than ordinary steel fibers in improving the crack resistance of concrete beams. Therefore, when studying the basic mechanical properties of concrete beams in the future, the full and reasonable use of recycled steel fibers can not only save resources and protect the environment, but also provide a new research direction for the green and sustainable development of building structures.

(2) The crack resistance of concrete beams increases with the increases of volume ratio of recycled

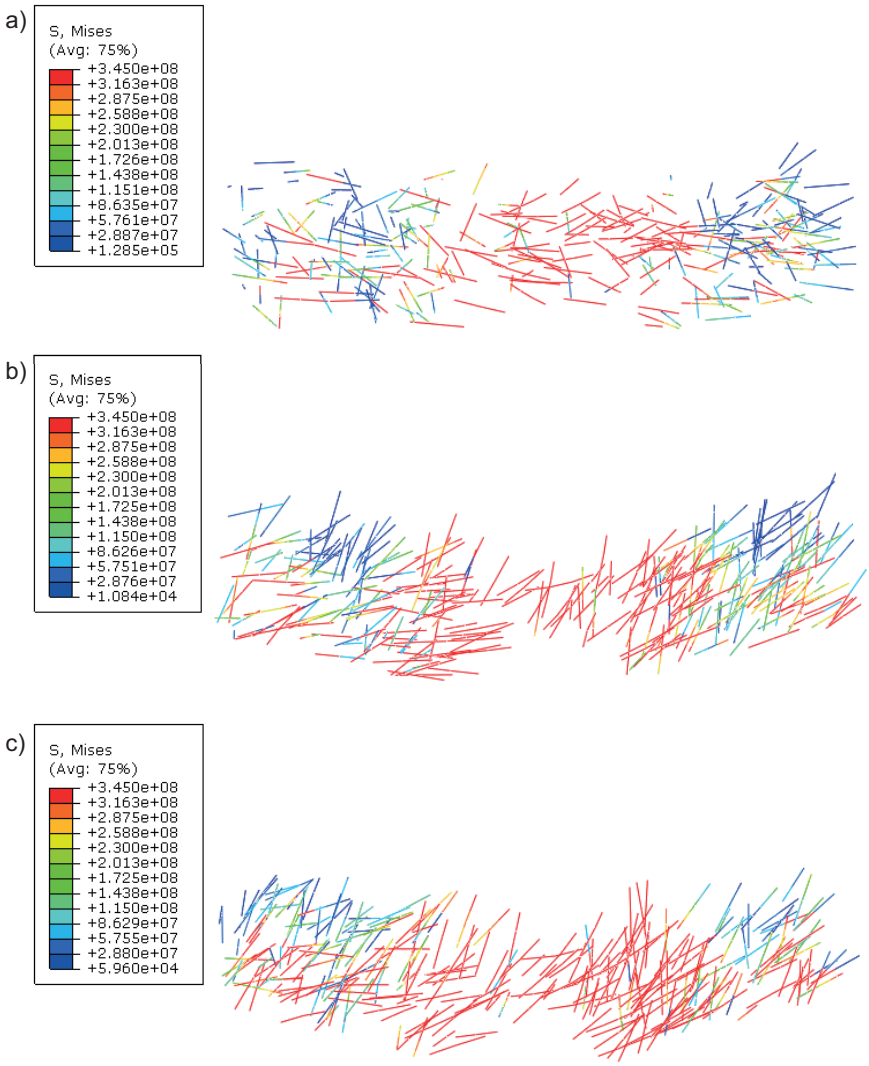

Fig. 17. The stress nephograms of recycled steel fibers with fiber length-diameter ratio of 50 at relative incision depth of 0.2, 0.3, and 0.4, a) (0.2); b) (0.3); c) (0.4).

TABLE IV. COMPARISONS BETWEEN THE LOAD CHARACTERISTIC VALUES AND UNSTABLE FRACTURE TOUGHNESS IN THE SIMULATION AND THOSE OF IN THE TEST.

Numbers	Test P_{ini}	Simulation P_{ini}	Test P_{max}	Simulation P_{max}	Test K^S_{IC}	Simulation K^S_{IC}
TPB-10-30-02	18.2	19.6	23.5	25.1	2.25	2.37
TPB-10-30-03	12.9	13.9	17.6	19.5	2.22	2.36
TPB-10-30-04	9.4	10.5	13.2	14.5	2.20	2.32
TPB-10-50-02	20.6	22.1	25.8	27.3	2.56	2.68
TPB-10-50-03	14.9	16.2	19.4	20.7	2.54	2.66
TPB-10-50-04	10.5	12.2	14.4	16.1	2.51	2.65
TPB-10-70-02	22.3	23.8	27.8	29.0	2.68	2.82
TPB-10-70-03	16.2	17.4	20.8	22.3	2.65	2.80
TPB-10-70-04	11.4	13.4	15.3	16.6	2.63	2.77

Note: Relative error =| measured value - simulated value |/ modulus ×100%.

steel fibers. When the fiber content is from 0.0% to 1.0%, the increased amplitude of the crack resistance of concrete beams increases gradually, and when the fiber content is from 0.5% to 1.0%, the increased amplitude of the crack resistance of concrete beams reaches the maximum. When the fiber content is from 1.0% to 1.5%, the increased amplitude of the crack resistance of concrete beams decreases. Therefore, in the future research, the recycled steel fibers with volume ratio of 1.5% can be added into concrete to improve the crack resistance of concrete beams, which also provides references for the recycling and utilization of wire from waste tires.

(3) The crack resistance of concrete beams increases with the increases of length-diameter ratio of recycled steel fibers. When the fiber length-diameter ratio is from 30 to 50, the crack resistance of concrete beams increases relatively large, and when the fiber length-diameter ratio is from 50 to 70, the crack resistance of concrete beams increases relatively small.

(4) The crack resistance of concrete beams decreases with the increases of relative incision depth of concrete beams. When the relative incision depth is from 0.2 to 0.3, the crack resistance of concrete beams decreases relatively large. When the relative incision depth is from 0.3 to 0.4, the crack resistance of concrete beams decreases relatively small.

(5) The equivalent fracture toughness of concrete beams does not change with the changes of relative incision depth and can be regarded as an inherent fracture property of the material itself (Fu and Chen 2017).

(6) The extended FEM in ABAQUS software was used to numerically simulate the fracture failure process and fracture performance of TPB beam specimens. The unstable fracture toughness of concrete beams was calculated and compared according to the simulation and test results, showing that most of simulated failure conditions correlate well with the experimental ones. However, some differences exist in the cracking speed and bending degree before fracture of TPB concrete beams and bending degree and macroscopic degree of cracks during the cracking process. The fracture behavior and reaction rules are consistent with the test, proving that the extended FEM is feasible to study the cracking behavior of various steel fiber-reinforced concrete beams in this experiment.

Prospects

In this study, several experiments were conducted to study the entire process from crack initiation to unstable expansion of TPB beam specimens under different control variables. Because of the limitation of test equipment and environmental conditions, and the immature design of parameters of specimens, some subjective and objective factors exist in the test process, causing some problems and deficiencies. The following two points are worth exploring in the future.

(1) In the test process, the TPB beams have only a specimen size of 550 mm × 150 mm × 150 mm. The size effect and the corresponding functional relationship of specimens have not been considered. The design of the size in future tests should be diversified, and the relationship between the fracture performance and size effect should be analyzed comprehensively (Zhang and Xu 2011).

(2) As for the numerical simulations of TPB beams, this test is limited to studying the cracking strain nephograms in the cracks propagation process, predominantly based on analyzing load characteristic values in the fracture performance. In future simulations, the macro responses of beams, such as the load-deflection curve, load-crack opening displacement curve, and energy field, can be further studied. Simultaneously, the extended FEM was adopted in this simulation, and more other simulation methods, such as the cohesion model, should be explored for comparative analysis.

DATA AVAILABILITY

The data supporting the findings of this study are included within the article.

CONFLICTS OF INTEREST

The authors declare that they have no conflict of interest.

ACKNOWLEDGMENT

This work was supported in part by the National Key Research and Development Program of China (No.2017YFC0806100) and the Jilin Scientific and Technological Planning Project (No.20200403161SF).

AUTHORS CONTRIBUTIONS

Theoretical analysis: Yan LI, Rong-Hua ZHAO. Numerical simulation: Wen-Yang DONG, Rong-Hua ZHAO. Experimental: Rong-Hua ZHAO, Geng CHEN. Experimental analysis: Rong-Hua ZHAO, Geng CHEN.

REFERENCES

Barros J.A.O., Figueiras J.A. (1999). Flexural behavior of SFRC: testing and modeling. Journal of Materials in Civil Engineering 11(4), 331-339. https://doi.org/10.1061/(ASCE)0899-1561(1999)11:4(331)

Cao P., Feng D.Ch., Cao Y.X. and Zuo W.X. (2013). Experimental study on fracture performance of notched beams of three-point bending fiber reinforced concrete. Engineering mechanics 30(S1), 221-225+231. https://doi.org/10.6052/j.issn.1000-4750.2012.05.S075

Carrillo J., Marriaga J.L., Baez F.A.L. (2020). Properties of steel fiber reinforced concrete using either industrial or recycled fibers from waste tires. Fibers and Polymers 21(9), 2055-2067. https://doi.org/10.1007/s12221-020-1076-1

Chbani H., Saadouki B., Boudlal M. and Barakat M. (2019). Determination of fracture toughness in plain concrete specimens by R curve. Fracture and Structural Integrity 13(49), 763-774. https://doi.org/10.3221/IGF-ESIS.49.68

Chen B., Liu N. (2014). Experimental research on properties of fresh and hardened rubberized concrete. Journal of Materials in Civil Engineering 26(8), 04014040. https://doi.org/10.1061/(ASCE)MT.1943-5533.0000923

Clerc G., Brunner A.J., Niemz P. and Kuilen J.W.V.D. (2020). Application of fracture mechanics to engineering design of complex structures. Procedia Structural Integrity 28, 1761-1767. https://doi.org/10.1016/j.prostr.2020.10.152

Fu Y., Chen Y.L. (2017). Experimental study on influence of relative incision depth on fracture properties of concrete. Journal of Water Resources and Water Engineering 28(04), 187-192. https://doi.org/10.11705/j.issn.1672-643X.2017.04.32

Huang B.S., Li G.Q., Pang S.S. and Eggers J. (2004). Investigation into waste tire rubber-filled concrete. Journal of Materials in Civil Engineering 16(3), 187-194. https://doi.org/10.1061/(ASCE)0899-1561(2004)16:3(187)

Lakavath C., Joshi S.S., Prakash S.S. (2019). Investigation of the effect of steel fibers on the shear crack-opening and crack-slip behavior of prestressed concrete beams using digital image correlation. Engineering Structures 193(AUG.15), 28-42. https://doi.org/10.1016/j.engstruct.2019.05.030

Li G., Cui S.S. (2020). A review on theory and application of plastic meso-damage mechanics. Theoretical and Applied Fracture Mechanics 109, 102686. https://doi.org/10.1016/j.tafmec.2020.102686

Li Y., Wang X.P., He Zh.G. and Fang Q. (2020). Experimental study on shear performance of industrial waste fiber reinforced cement matrix composites. Industrial Building 50(12), 88-92+159. https://doi.org/10.13204/j.gyjzG19100806

Li Z.X., Liu Y.G. (2006). Practical analytical method for solving equivalent fracture toughness of concrete based on virtual crack model. Engineering Mechanics 2006(11), 91-98. https://doi.org/CNKI:SUN:GCLX.0.2006-11-015

Liao L., Zhao J., Zhang F., Li Sh.Q. and Wang Zh.H. (2020). Experimental study on compressive properties of SFRC under high strain rate with different fiber content and aspect ratio. Construction and Building Materials 261, 119906. https://doi.org/10.1016/j.conbuildmat.2020.119906

Liu Q., Looi T.W., Chen H.H., Tang C. and Su R.K.L. (2020). Framework to optimise two-dimensional DIC measurements at different orders of accuracy for concrete structures. Structures 28, 93-105. https://doi.org/10.1016/j.istruc.2020.08.056

Liu S.G., Bai R., Yan C.W. and Deng Y.H. (2018). Experimental study and theoretical calculation of bending stiffness of reinforced fiber reinforced cement matrix composite beams. Journal of Building Structures 39(S2), 176-182. https://doi.org/10.14006/j.jzjgxb.2018.S2.024

Ming M., Zheng S.S., Zheng H., He J.Ch., Dong L.G. and Song M.Ch. (2020). Experimental study on bond slip behavior of profile steel high performance fiber reinforced concrete. Engineering Mechanics 37(08), 148-157. https://doi.org/10.6052/j.issn.1000-4750.2019.09.0555

Nourmohammadi N., O'Dowd N.P., Weaver P.M. (2020). Effective bending modulus of thin ply fibre composites with uniform fibre spacing. International Journal of Solids and Structures 196–197, 26-40. https://doi.org/10.1016/j.ijsolstr.2020.04.004

Peng G.F., Niu X.J., Long Q.Q. (2015). Experimental study of strengthening and toughening for recycled steel fiber reinforced ultra-high performance concrete. Key Engineering Materials 629-630, 104-111. https://doi.org/10.4028/www.scientific.net/KEM.629-630.104

Raju R.A., Lim S., Akiyama M. and Kageyama T. (2020). Effects of concrete flow on the distribution and orientation of fibers and flexural behavior of steel

fiber-reinforced self-compacting concrete beams. Construction and Building Materials 262, 119963. https://doi.org/10.1016/j.conbuildmat.2020.119963

Ren X., Li J. (2013). Multi-scale based fracture and damage analysis of steel fiber reinforced concrete. Engineering Failure Analysis 35, 253-261. https://doi.org/10.1016/j.engfailanal.2013.01.029

Simalti A., Singh A.P. (2021). Comparative study on performance of manufactured steel fiber and shredded tire recycled steel fiber reinforced self-consolidating concrete. Construction and Building Materials 266(2017), 121102. https://doi.org/10.1016/j.conbuildmat.2020.121102

Skaryński, Kozicki J., Tejchman J. (2013). Application of DIC technique to concrete—study on objectivity of measured surface displacements. Experimental Mechanics 53(9), 1545-1559. https://doi.org/10.1007/s11340-013-9781-y

Sun X.J., Gao Z., Cao P., Zhou C., Ling Y., Wang X., Zhao Y. and Diao M. (2019). Fracture performance and numerical simulation of basalt fiber concrete using three-point bending test on notched beam. Construction and Building Materials 225(Nov.20), 788-800. https://doi.org/10.1016/j.conbuildmat.2019.07.244

Tang Y.X., Chen H.N. (2018). Simulation of crack propagation in concrete based on extended finite element method. Key Engineering Materials 783, 165-169. https://doi.org/10.4028/www.scientific.net/KEM.783.165

Xia P.X., Zou G.P., Tang L.Q. (2011). Numerical simulation on the compound crack propagation process in concrete. Advanced Materials Research 250-253, 1139-1142. https://doi.org/10.4028/www.scientific.net/AMR.250-253.1139

Xu S.L., Yu X.L., Li Q.H. (2015). Determination of crack initiation and equivalent crack length of low strength concrete by electric measurement. Engineering Mechanics 32(12), 84-89. https://doi.org/CNKI:SUN:GCLX.0.2015-12-012

Xu S.L., Zhao Y.H. (2008). Fracture process criterion and analysis of crack propagation of concrete. Engineering Mechanics 25(S2), 20-33. https://doi.org/CNKI:SUN:GCLX.0.2008-S2-005

Yin Y.Y., Hu S.W., Wang Y.H. (2019). Influence of dead weight on fracture behavior of three-point bending concrete beams. Engineering Mechanics 36(07), 48-56+108. https://doi.org/CNKI:SUN:GCLX.0.2019-07-008

Zhang X.F., Xu S. (2011). A comparative study on five approaches to evaluate double-K fracture toughness parameters of concrete and size effect analysis. Engineering Fracture Mechanics 78(10), 2115-2138. https://doi.org/10.1016/j.engfracmech.2011.03.014